# The goya mouse mutant reveals distinct newly identified roles for MAP3K1 in the development and survival of cochlear sensory hair cells

DMM Advance Online Articles. Posted 5 November 2015 as doi: 10.1242/dmm.023176
Access the most recent version at http://dmm.biologists.org/lookup/doi/10.1242/dmm.023176

# The *goya* mutation identifies distinct novel roles for MAP3K1 in cochlear sensory hair cell development and survival

Andrew Parker[1], Sally H. Cross[2], Ian J. Jackson[2,3], Rachel Hardisty-Hughes[1], Susan Morse[1], George Nicholson[1,4], Emma Coghill[1] Michael R. Bowl[1] and Steve D.M. Brown[1]*

[1]MRC Mammalian Genetics Unit, MRC Harwell, OX11 0RD, UK

[2]MRC Human Genetics Unit, MRC IGMM, University of Edinburgh, Edinburgh, Scotland, UK

[3]The Roslin Institute, University of Edinburgh, Easter Bush, UK

[4]Department of Statistics, University of Oxford, UK

*To whom correspondence should be addressed: s.brown@har.mrc.ac.uk

**Keywords**

MAP3K1, supernumerary outer hair cells, cochlear development, sensory hair cell survival, hearing loss.

**Summary Statement**

The ENU derived mouse mutant, *goya*, for the first time reveals multiple roles of MAP3K1 in cochlear development and correct auditory function.

**Abstract**

The Mitogen-Activated Protein kinase, MAP3K1, plays an important role in a number of cellular processes, including epithelial migration during eye organogenesis. In addition, studies in keratinocytes indicate that MAP3K1 signaling through JNK is important for actin stress fibre formation and cell migration. However, MAP3K1 can also act independently of JNK in the regulation of cell proliferation and apoptosis.

We have identified a mouse mutant, *goya*, which exhibits eyes-open-at-birth and microphthalmia phenotypes. In addition, these mice also have hearing loss. The *goya* mice carry a splice site mutation in the *Map3k1* gene. We show that *goya* and kinase-deficient *Map3k1* homozygotes initially develop supernumerary cochlear outer hair cells (OHCs) that subsequently degenerate, and a progressive profound hearing loss is observed by 9-weeks of age. Heterozygote mice also develop supernumerary OHCs, but no cellular degeneration or hearing loss is observed. MAP3K1 is expressed in a number of inner ear cell types, including outer and inner hair cells, stria vascularis and spiral ganglion. Investigation of targets downstream of MAP3K1 identified an increase in p38 phosphorylation (Thr180/Tyr182) in multiple cochlear tissues. We also show the extra OHCs do not arise from aberrant control of proliferation via p27KIP1.

The identification of the *goya* mutant reveals a novel signaling molecule involved with hair cell development and survival. Mammalian hair cells do not have the ability to regenerate after damage, which can lead to irreversible sensorineural hearing loss. Given the observed *goya* phenotype, and the many diverse cellular processes MAP3K1 is known to act upon, further investigation of this model may help elaborate

upon the mechanisms underlying sensory hair cell specification, and pathways important for their survival. In addition, MAP3K1 is revealed as a new candidate gene for human sensorineural hearing loss.

## Introduction

The signalling pathways underlying epithelial sheet movements are well studied, and have identified the Mitogen-Activated Protein (MAP) kinase, MAP3K1 as having an important role in this process (Takatori et al., 2008; Xia and Kao, 2004; Zhang et al., 2005; Zhang et al., 2003). In mice, loss-of-function mutations in the *Map3k1* gene lead to defects in epithelial migration that manifest as an eyes-open-at-birth phenotype (Xia and Kao, 2004; Zhang et al., 2003), due to defects in actin polymerisation and c-JUN phosphorylation. Studies in keratinocytes demonstrate that activation of c-Jun N-terminal kinase (JNK) by TGF-beta and Activin requires MAP3K1, leading to c-JUN phosphorylation, actin stress fibre formation and cell migration (Zhang et al., 2005; Zhang et al., 2003). Whilst it is clear a MAP3K1-JNK cascade is critical for epithelial sheet movements during eye organogenesis, it may also be expected to have a role in the development of other epithelia. Indeed, MAP3K1 is required during wound healing where injury up-regulates MAP3K1 and leads to changes in the expression of genes associated with extracellular matrix homeostasis. Conversely, knock-down of MAP3K1 impairs wound healing (Deng et al., 2006). MAP3K1 has also been shown to act independently of JNK during the regulation of cell proliferation and apoptosis in the retina (Mongan et al., 2011).

In humans, *MAP3K1* mutations have been shown to cause 46,XY disorders of sexual development (DSD) (Loke et al., 2013; Pearlman et al., 2010). A number of these mutations have been studied, and they all result in the increased phosphorylation of downstream MAPK proteins p38 MAPK and ERK1/2.

As part of an *N*-ethyl-*N*-nitrosourea (ENU) mutagenesis recessive screen we have identified a mouse mutant, *goya*, which carries a mutation in the *Map3k1* gene. The mutant was identified by its eyes-open-at-birth (EOB) phenotype, and also by the reduction or absence of a response to a Click-box test indicating hearing loss. Homozygous *goya* mice initially develop supernumerary outer hair cells (OHCs) in the inner ear, widespread OHC degeneration is observed by 4-weeks of age, and the mice are profoundly deaf by 9-weeks of age. This identifies a novel role for MAP3K1 in auditory hair cell development and survival. Characterisation of the *goya* mutant provides an opportunity to elaborate upon the requirement of this Mitogen-Activated Protein kinase in cochlear organogenesis and maintenance.

## Results

### Identification of a mouse mutant with eye, vision and auditory defects

The *goya* mouse mutant was identified, from a recessive ENU-mutagenesis phenotype-driven screen, as having eyes-open-at-birth (EOB) (see supplementary material Fig. S1A). In the adult EOB mice, eye pathology is highly variable, ranging from microphthalmic, to apparently normal, to bulging (see supplementary material Fig. S1B ). However, all EOB mice failed to respond in an optokinetic drum visual function assay (data not shown). Rosetting was observed in the retinal layers, although at P0 the structure of tight junctions and the outline of retinal pigment epithelium (RPE) cells appeared normal (see supplementary material Fig. S1C). Additionally, these mice also had a reduced Preyer's response to a Click-box auditory stimulus. Given the interesting combination of eye and auditory defects, we proceeded to identify the *goya* mutation and further explore the deafness phenotype.

### *goya* is caused by a point mutation in the *Map3k1* gene

Using SNP-based mapping the *goya* phenotype was localized to a 24.7 Mb region on chromosome 13 between SNPs rs13481942 and rs6316705. Within the interval there was a strong candidate, *Map3k1*, with mice deficient for this gene having previously been shown to display EOB (Juriloff et al., 2004; Yujiri et al., 2000; Zhang et al., 2003). There have been no reports of hearing loss in *Map3k1* mouse models. *Map3k1* is highly expressed in the migrating leading edge of the eyelid epithelium and it is thought that in its absence the migration of these cells is impaired leading to the failure of eyelid closure during embryogenesis (Xia and Kao, 2004; Zhang et al., 2005; Zhang et al., 2003). Investigation of a kinase-deficient *Map3k1*$^{tm1Yxia/tm1Yxia}$ allele showed that retinal phenotypes including increased proliferation and subsequent

apoptosis of Müller glial cells were due to a pathway separate to eyelid closure, highlighting the multiple roles of MAP3K1 in cellular development and survival (Mongan et al., 2011).

Sanger sequencing of the *Map3k1* gene exons and intron/exon boundaries revealed a single nucleotide change in the intron 13 splice donor site (IVS13+2T>C) of affected mice (Fig. 1A). To ascertain the effect of the *goya* mutation on splicing we performed RT-PCR analysis of RNA isolated from postnatal day 1 (P1) organ of Corti dissected from *goya* littermate mice. For *Map3k1*$^{+/+}$, the expected product of 341bp was obtained (Fig. 1B). However, for *Map3k1*$^{goya/goya}$ the wild-type product was absent and two smaller products could be seen (Fig. 1B). Sanger sequencing of the *Map3k1*$^{+/+}$ RT-PCR product shows exons 12, 13 and 14 correctly spliced, whereas sequencing of the two *Map3k1*$^{goya/goya}$ products show aberrant splicing (Fig. 1C). The more abundant mutant product (*Map3k1*$^{goya/goya}$ RT-PCR 1) demonstrates the use of a cryptic splice donor site within exon 13 (Fig. 1C). In this case 81 nucleotides are skipped leaving the transcript in-frame, but producing a protein with an internal deletion of 27 amino acids. The less abundant mutant product (*Map3k1*$^{goya/goya}$ RT-PCR 2) shows complete skipping of exon 13 (190 nucleotides) with exon 12 spliced directly to exon 14 (Fig. 1C). Translation of this transcript would lead to the production of a protein containing the first 723 amino acids of MAP3K1 followed by a frame-shift and the incorporation of seven novel amino acids before a stop codon is encountered. If produced this truncated protein would lack the C-terminal 770 amino acids of MAP3K1 including the kinase domain.

**The *goya* mutant is severely deaf**

To confirm *Map3k1* as the causative gene we mated mice carrying the *goya* mutation to mice carrying the *Map3k1*$^{tm1Yxia}$ allele. We performed auditory brainstem response (ABR) analysis on both *Map3k1*$^{goya}$ and *Map3k1*$^{tm1Yxia}$ heterozygote and homozygote mice as well as compound heterozygote and wild-type mice. At 9-weeks of age, *Map3k1*$^{goya/+}$ and *Map3k1*$^{tm1Yxia/+}$ heterozygous mice have normal auditory thresholds similar to wild-type (*Map3k1*$^{+/+}$) mice. Whereas, both *Map3k1*$^{goya/goya}$ and *Map3k1*$^{tm1Yxia/tm1Yxia}$ homozygotes show a significant hearing loss with average ABR thresholds of ~80 dB SPL across all frequencies tested ($p=<0.0001$) (Fig. 2C). Importantly, the compound heterozygous mice (*Map3k1*$^{goya/tm1Yxia}$) also have elevated ABR thresholds similar to those of homozygote mice. Failure of these models to complement confirms that the ENU-induced *Map3k1* mutation underlies the *goya* phenotype. To investigate the onset of hearing loss, we performed ABR testing of homozygote and wild-type mice at 2- and 4-weeks of age. At 2-weeks of age, *Map3k1*$^{goya/goya}$ mice have ABR thresholds similar to those of wild-type mice at all but the highest frequency tested (26kHz), whereas *Map3k1*$^{tm1Yxia/tm1Yxia}$ mice show elevated thresholds at all frequencies tested (Fig. 2A). At 4-weeks of age, both homozygous mutants exhibit significantly elevated ABR thresholds (+30-40dB) at all frequencies tested when compared to wild-type controls (Fig. 2B).

To determine the longitudinal effects of the *goya* mutation on hearing function we performed ABR on mice at 1-year of age. *Map3k1*$^{goya/+}$ mice have ABR thresholds similar to those of wild-type mice, demonstrating *goya* heterozygotes do not develop late-onset hearing loss (Fig. 2D). Moreover, there is no further decline in auditory function of *Map3k1*$^{goya/goya}$ animals between 9-weeks and 1-year (Fig. 2C,D). To

investigate vestibular effects of the mutation, we performed swim tests on 1-year old *Map3k1*$^{goya/goya}$ mice and no overt vestibular dysfunction was observed.

**Hair cell abnormalities in the *Map3k1* mutants**

Given the elevated auditory thresholds of *Map3k1*$^{goya/goya}$ and *Map3k1*$^{tm1Yxia/tm1Yxia}$ mice, we proceeded to examine in detail the ears of these mice. H&E staining of cochlear sections suggest cellular degeneration within the organ of Corti of 9-week old homozygote mice, however other inner ear structures such as Reissner's membrane, stria vascularis and spiral ganglion neurons (SGN) appear normal (data not shown). Additionally, no defects in middle ear morphology were observed. To further assess the organ of Corti we used scanning electron microscopy (SEM) to examine the ultrastructure of the sensory epithelium. At 2-weeks of age, *Map3k1*$^{goya/goya}$ and *Map3k1*$^{tm1Yxia/tm1Yxia}$ mice show a normal cellular arrangement of the sensory epithelium with the exception that both mutants have more OHCs than wild-type (Fig. 3A). The additional OHCs are organised as an extra row that extends largely throughout the cochlear regions examined (Fig. 3A). However, by 4-weeks of age both mutants show degeneration of OHCs with an increasing severity from apex-to-base (Fig. 3B). By 9-weeks of age both mutants show further degeneration. Conversely, no OHC loss is observed in wild-type mice by 9-weeks of age (Fig. 3C). At 2-, 4- and 9-weeks of age inner hair cell (IHC) morphology appeared normal in all except *Map3k1*$^{tm1Yxia/tm1Yxia}$ cochlea at 9-weeks, which showed a slight reduction in number again with an apical-to-basal gradient (Fig. 3C). Although at 9-weeks of age the majority of IHCs were unaffected, the extent of degeneration in small patches of the *Map3k1*$^{tm1Yxia/tm1Yxia}$ organ of Corti was very severe. IHCs, OHCs and pillar cells had disappeared and rosette-like formations of what appear to be Claudius and

Hensen cells had formed in their place (Fig. 3D). A similar pattern of cellular remodelling has been previously noted, in post aminoglycoside damaged cochlea (Taylor et al., 2012). Interestingly, similar to homozygous mutants, *Map3k1*$^{goya/+}$ and *Map3k1*$^{tm1Yxia/+}$ mice also display extra OHCs compared to wild-type mice, but unlike homozygous mutants no OHC degeneration was observed at any time-point (Fig. 3E). Further investigation shows that similar to wild-type the heterozygote mutants have episodic patches of extra OHCs. However, unlike wild-type the heterozygote mutants show an increase in the occurrence of extra rows of OHCs, present in 43%, 27% and 4% of images from *Map3k1*$^{tm1Yxia/+}$, *Map3k1*$^{goya/+}$ and wild-type mice, respectively (Fig. 3F). These data suggest roles for MAP3K1 in sensory hair cell development and survival.

To assess the progressive nature of cell loss in the different regions of the cochlear spiral, and to allow comparison between genotypes, sensory cell counts were performed. At 2- and 4-weeks of age, IHC numbers were similar between *Map3k1*$^{+/+}$, *Map3k1*$^{goya/goya}$ and *Map3k1*$^{tm1Yxia/tm1Yxia}$ mice. At 9-weeks of age IHC numbers were similar between *Map3k1*$^{+/+}$ and *Map3k1*$^{goya/goya}$ mice, but a trend for reduced numbers of IHCs in the basal region of *Map3k1*$^{tm1Yxia/tm1Yxia}$ cochleae was observed (Fig. 4A,B,C). Up to 9-weeks of age, *Map3k1*$^{+/+}$ mice show consistent numbers of OHCs across the different regions of the cochlea (Fig. 4D). At 2-weeks of age, *Map3k1*$^{goya/goya}$ and *Map3k1*$^{tm1Yxia/tm1Yxia}$ mice have increased numbers of OHCs compared to wild-type, which is significant for most of the regions assessed (Fig. 4D,E,F). At 4-weeks of age, degeneration of OHCs progressed in *Map3k1*$^{goya/goya}$ and *Map3k1*$^{tm1Yxia/tm1Yxia}$ mice. In the apical, mid-apical, mid, and mid-basal regions of the cochlear spiral, *Map3k1*$^{goya/goya}$ mutants show an average reduction in OHC numbers

of 26%, 24%, 70%, 95%, respectively, while *Map3k1*$^{tm1Yxia/tm1Yxia}$ mutants show reductions of 20%, 43%, 67%, 96%, respectively (Fig. 4E,F). A similar apical-to-basal increase in severity is also observed in 9-week old mutants (Fig. 4).

To determine statistical significance, the rate of hair cell loss was estimated under a Poisson generalized linear model (see Methods). There was no statistical support for IHC loss in any genotypic group (See supplementary material Table S1&S2). There was strong statistical support for OHC loss in the *Map3k1*$^{goya/goya}$ and *Map3k1*$^{tm1Yxia/tm1Yxia}$ genotypic groups (but no evidence in the wild-type group; See supplementary material Table S2). The rate of OHC loss in the mutant groups increased consistently from apical-to-basal turns (See supplementary material Table S1). The rate of OHC loss did not differ significantly between the two mutant groups. These statistical analyses quantify and corroborate the obvious effects visible in Figure 3.

**Localisation of MAP3K1 to the inner ear**

Commercially available anti-MAP3K1 antibodies have poor specificity, therefore we utilized the *Map3k1*$^{tm1Yxia}$ allele which produces a MAP3K1-ß-Galactosidase fusion protein (Xia et al., 2000; Zhang et al., 2003). Using X-Gal staining, widespread expression of MAP3K1-ß-Galactosidase was observed in *Map3k1*$^{tm1Yxia/tm1Yxia}$ cochleae (Fig. 5A). Closer examination of the cochlear duct showed staining in IHCs and OHCs, border cells of the internal spiral sulcus, Claudius and Hensen cells as well as SGN (Fig. 5C). No labelling was observed in wild-type cochleae (Fig. 5B,D). Histological sections confirm the whole-mount localisation data and also reveal expression in cell types such as Deiters' cells, pillar cells, Reissner's membrane,

marginal cells in the stria vascularis and the tympanic border cells of the basilar membrane (Fig. 5E,G,O,P). A transverse section of the organ of Corti also highlighted the expression of the fusion protein in IHCs and OHCs (Fig. 5Q). In addition to the expression in the cochlea, staining was observed in the vestibular system, including the apical surface of supporting cells and hair cells in both otolithic organs and the cristae of the semi-circular canals (Fig. 5I,K,M). Positive staining in all *Map3k1*$^{tm1Yxia/+}$ samples mirrored that of homozygotes, whereas no staining was seen in either the vestibular system or cochleae of *Map3k1*$^{+/+}$ mice (Fig. 5F,H,J,L,N).

**Aberrant proliferation is not the cause of supernumerary OHC in *Map3k1* mutant mice**

The cyclin-dependent kinase inhibitor, *p27*$^{Kip1}$, is a key regulator that arrests the cell cycle at G1. Its expression in the developing cochlea produces a zone of non-proliferation (ZNP) and these cells subsequently differentiate into sensory hair cells and supporting cells. It is known that these ZNP cells undergo their final division by embryonic day 14.5 (E14.5). However, in *p27*$^{Kip1}$ homozygous null mice, there is an extended period of pro-sensory precursor cell proliferation leading to increased numbers of hair cells and supporting cells (Lowenheim et al., 1999). We used 5-ethynyl-2'-deoxyuridine (EdU) to investigate if proliferation was increased or extended in the developing *Map3k1*$^{tm1Yxia/tm1Yxia}$ mutant cochlea. In addition we used an anti-p27KIP1 antibody to investigate for possible regulatory defects associated with a MAP3K1 deficiency. Figure 6 shows that p27KIP1 localisation is unaffected in the *Map3k1*$^{tm1Yxia/tm1Yxia}$ cochlea at E14.5 (Fig. 6A,B), and the lack of EdU-positive nuclei in the region of the cochlea duct positively immuno-labelled for p27KIP1 indicates the ZNP is established correctly. At E18.5, we again found no difference in

localisation of p27KIP1 in mutant cochleae. Moreover, no increase in the number of proliferating cells was seen in the cochlear duct of *Map3k1*$^{tm1Yxia/tm1Yxia}$ mice compared to *Map3k1*$^{+/+}$ littermate controls (Fig. 6C,D,E,F,G,H). Together these data suggest that increased or extended proliferation of pro-sensory precursor cells is not the cause of extra OHCs in *Map3k1* mutant mice.

**The *goya* mutation in *Map3k1* results in an increase of p38 phosphorylation in P1 mouse inner ears**

To investigate the effects of the *goya* mutation on MAPK pathway targets we used both gene expression and immunodetection strategies. We extracted RNA from isolated P1 cochlear ducts and performed qRT-PCR to investigate expression of *Map3k1* and genes likely to be involved in MAP3K1 signalling (*Ccna1* (*Cyclin A1*), *Ccnd1* (*Cyclin D1*), *Lgr5*, *Dhfr*, *Axin2*, *Ctnbb1* (*β-catenin*), *E2f1*, *Rb1*) (Loke et al., 2013; Mongan et al., 2011). In addition, expression of JNK targets, *Jun* and *Fos* were also analysed. Although some differences observed between genotypes, we did not see any notable fold changes in expression of any of the genes investigated (see supplementary material Fig. S2A).

As MAP3K1 has been shown to be involved with activation of all three major MAPK pathways, ERK, JNK and p38 MAPK, we investigated the phosphorylation of these downstream target proteins. Protein lysates from P1 inner ears were analysed for both total and phosphorylated ERK1/2, JNK and p38 MAPK. Moreover, given the effects in the eye of *Map3k1* mutations on RB phosphorylation (see above), we also assessed total and phospho-RB levels. No differences in phosphorylation were detectable in

ERK1/2, JNK or RB. However, a trend towards increased p38 phosphorylation in *Map3k1*$^{goya/goya}$ inner ear lysates was observed (Fig. 7A).

To further investigate p38 MAPK phosphorylation in *Map3k1*$^{goya/goya}$ inner ears, we performed immunohistochemistry on sections from P1 mice (Fig. 7B). Anti-phospho-p38 labelling of *Map3k1*$^{goya/goya}$ homozygotes showed intense nuclear staining of all cell types in the cochlea duct and SGN (Fig. 7Biii,Biv). The majority of nuclei in the surrounding structures such as the spiral ligament and spiral limbus were also intensely stained. Labelling of *Map3k1*$^{+/+}$ mice displayed a similar pattern of nuclear expression, however under identical experimental conditions the staining was much weaker and fewer nuclei in the surrounding structures stained positive for phospho-p38 MAPK (Fig. 7Bi,Bii).

We quantified the difference in anti-phospho-p38 staining using the imageJ plugin, ImmunoRatio, analysing mid-cochlear sections from *Map3k1*$^{goya/goya}$ and *Map3k1*$^{+/+}$ mice. ImmunoRatio has been designed to diagnostically assess the percentage area of positively DAB stained nuclei in a given sample, however the analysis does not take into account intensity of stain. The results show a significant ($p=0.0126$) increase in positive nuclear area in *Map3k1*$^{goya/goya}$ mice (n=3) when compared with *Map3k1*$^{+/+}$ (n=2) (Fig. 7C).

We also performed immunohistochemistry with anti-phospho-JNK and anti-phospho-ERK1/2 antibodies (Fig. 7D,E), and consistent with our Western data no obvious differences in intensity or expression pattern were observed between *Map3k1*$^{goya/goya}$ and *Map3k1*$^{+/+}$ mice. It is worth noting that these antibodies show strong labelling beneath the basal surface of the IHC and OHC, consistent with the location of SGN

neurite extensions at the P1 time point. In addition low-level anti-phospho JNK was detected in the cytoplasm and nucleus of cells throughout the organ of Corti of both *Map3k1*$^{goya/goya}$ and *Map3k1*$^{+/+}$ mice.

## Discussion

We report that an IVS13+2T>C ENU-induced lesion in *Map3k1* is the causative mutation underlying both the EOB and auditory phenotypes in the *goya* mutant. These findings demonstrate a new role for MAP3K1 in auditory function. Similar findings are reported in the parallel study (Yousaf et al., 2015). Mice homozygous for the *goya* mutation and *Map3k1* null mice each develop supernumerary OHCs, and both show a progressive decline in auditory function resulting in severe hearing loss by 9-weeks of age. The *goya* mutant showed a slower rate of auditory decline, but this is likely due to the different genetic backgrounds of the two mutants, with *goya* crossed to C3H and *tm1Yxia* crossed to C57BL/6J. Apart from the early auditory thresholds, no major differences in phenotype were noted between the *goya* and the *tm1Yxia* alleles. Ultrastructural examination of $Map3k1^{goya/goya}$ and $Map3k1^{tm1Yxia/tm1Yxia}$ mutant cochleae, uncovered a progressive cellular degeneration in the organ of Corti with an apical-to-basal increase in severity. Cellular loss was first seen in the OHCs, although by 9-weeks IHCs and pillar cells were also missing in some mid and mid-basal regions, although not statistically significant. Mice heterozygous for either the $Map3k1^{goya}$ or the $Map3k1^{tm1Yxia}$ allele also develop extra OHCs, but interestingly they do not show progressive cellular degeneration as seen in the respective homozygotes. Indeed, at 1-year of age $Map3k1^{goya/+}$ and wild-type mice have similar auditory thresholds. These data suggest that within the organ of Corti MAP3K1 plays multiple roles in cellular development and survival.

We show that MAP3K1 is widely expressed in the inner ear. The expression in OHCs and IHCs, along with Deiters' cells, in the organ of Corti is consistent with the

observed phenotype of additional rows of OHCs and OHC degeneration that we observe in *Map3k1* mutants. Our findings of MAP3K1 expression in the cochlea are consistent with the observations of Yousaf et al. (2015) in that they too report expression in Deiters' cells, Reissner's membrane and the stria vascularis. However, we identified some additional sites of expression including Claudius cells, Hensen cells and Border cells, as well as the basilar membrane. We also observed expression at the apical surface of the vestibular sensory epithelia, however no overt vestibular dysfunction was detected in either homozygous mutant. It is possible that the normal vestibular function in these mice is a consequence of functional redundancy between MAP3K1 and other MAP3Ks. For example MAP3K4 is known to activate the same downstream pathways as MAP3K1 (Morrison, 2012).However, a previous study investigating the role of MAP3Ks in testis determination failed to uncover functional redundancy between MAP3K1 and MAP3K4 (Warr et al., 2011).

The *goya* mutation has led to the identification of a new sensorineural deafness locus and it is important to consider *Map3k1* as a candidate gene for both dominant and recessive human deafness loci. Human mutations in *MAP3K1* have been shown to cause 46,XY disorders of sex development (DSD) (Pearlman et al., 2010). Two mutations, including a splice-acceptor mutation and a missense mutation, were identified in two families with 46,XY DSD. Moreover, a further two missense mutations were found in 11 sporadic cases examined. For three of these mutations MAP3K1 function was studied, including phosphorylation of downstream targets p38, ERK1/2 and JNK. Two of the mutations increased activation of p38 and ERK, possibly resulting from enhanced binding of RHOA to MAP3K1. However, there are no reports of hearing impairment for any of the individuals carrying MAP3K1

mutations. A possible explanation for the absence of an auditory phenotype in *Map3k1*-related 46,XY DSD patients is that they are heterozygous for these mutations; homozygous loss-of-function MAP3K1 mutations in human may not be viable. We investigated downstream pathways of MAP3K1 in the inner ear of P1 *Map3k1*$^{goya/goya}$ mice and observed an increase in p38 phosphorylation, but we did not see any differences in ERK1/2 phosphorylation.

Mice lacking retinoblastoma protein develop extra inner and outer hair cells, and analysis of progenitor cell proliferation indicates that RB1 is involved in cell cycle exit of sensory progenitor cells (Sage et al., 2005). The additional hair cells in *Rb1* knockout mice can transduce mechanical stimuli, but they undergo apoptosis and are completely missing by 3-months of age (Sage et al., 2006). Similarly, mice lacking p27KIP1, an inhibitor of cyclin-dependent kinases, also develop supernumerary sensory hair cells (Lowenheim et al., 1999). Given the close similarities of the *Map3k1* mutant inner ear phenotype to that seen in *Rb1* and *p27*$^{kip1}$ mutants and the reported effects of a *Map3k1* knockout on *Rb1* signalling in the retina, we surmised that the effects on OHCs observed in both the *Map3k1*$^{goya}$ and *Map3k1*$^{tm1Yxia}$ mutants are due to a JNK independent pathway, likely the RB/E2F pathway. However, at the P1 time point investigated we found no significant changes in the levels of cyclin D1 and CDKs, the downstream effectors of p27KIP1 or in phosphorylation levels of RB1 protein. Moreover we observed no difference in localisation of the anti-proliferative marker p27KIP1 in the developing cochleae of *Map3k1*$^{tm1Yxia/tm1Yxia}$ mice and littermate controls. Indeed an absence of EdU positive nuclei within the pro-sensory region of *Map3k1*$^{tm1Yxia/tm1Yxia}$ cochleae at E14.5 confirms the ZNP is correctly established in these mice. At E18.5 the continued absence of EdU positive nuclei

within the sensory cell domain indicates that the p27KIP1-induced cell cycle arrest is maintained in *Map3k1*$^{tm1Yxia/tm1Yxia}$ cochleae. These findings suggest that the supernumerary OHCs found in MAP3K1-deficient cochleae do not arise as a consequence of extended or aberrant proliferation of pro-sensory progenitor cells. MAP3K1 is known to act upon a diverse number of molecular pathways, many of which affect cellular proliferation and transcriptional regulation. It is possible that a reduction in MAP3K1 activity leads to dysregulation of genes or proteins involved with cellular fate within the sensory epithelium, or those required for the correct establishment of cell fate boundaries, potentially resulting in additional OHCs. As such, further investigation of the mechanism underlying the auditory phenotype identified in the *goya* mice will require additional transcriptomic and proteomic studies.

In conclusion, we show that in addition to previously reported eye phenotypes resulting from MAP3K1 deficiency, both heterozygous and homozygous *goya* and *Map3k1* null mutant mice initially develop supernumerary cochlear OHCs. In homozygous, but not heterozygous mutants, OHCs progressively degenerate and mice are severely deaf by 9-weeks of age. These phenotypic differences indicate that MAP3K1 may play distinct roles in cochlear development and hair cell survival. We show increased p38 phosphorylation in the cochleae of *goya* homozygote mice, and EdU studies reveal the extra OHCs result from a mechanism other than aberrant proliferation. Characterization of *goya* reveals a novel signalling molecule involved with mammalian audition, and identifies a new candidate gene for human sensorineural hearing loss.

## Methods

### *Mice*

All animals were housed and maintained under specific pathogen-free (SPF) conditions in individually ventilated cages in the Mary Lyon Centre, MRC Harwell, in adherence to environmental conditions as outlined in the Home Office Code of Practice. Animal procedures were carried out in line with Home Office regulations, and mice were euthanized by Home Office Schedule 1 methods.

The *goya* mutant line was identified from the collaborative ENU mutagenesis vision screen undertaken by MRC MGU Harwell and MRC HGU Edinburgh. ENU-treated $G_0$ C57BL/6 male mice were mated to C3H.C-*Pde6b*$^+$ female mice to produce $G_1$ progeny. $G_1$ males were mated to C3H.C-*Pde6b*$^+$ female mice to produce $G_2$ progeny. Female $G_2$ mice were backcrossed to the $G_1$ fathers to produce $G_3$ mice that were screened for recessively inherited phenotypes. The *goya* line was maintained on a C3H genetic background by outcrossing and intercrossing successive generations. MAP3K1 null mice (*Map3k1*$^{tm1Yxia/tm1Yxia}$) were imported from Ying Xia's group at the University of Cincinnati College of Medicine (Cincinnati, USA) and rederived by *in vitro* fertilisation by the FESA core in the Mary Lyon Centre to maintain SPF status. The null mice were backcrossed to C57BL/6J.

### *Histological analysis (Supplemental data figure S1)*

Animals were euthanized and eyes fixed in Davidson's fixative. Fixed specimens were decalcified, dehydrated and embedded in paraffin wax, 5µm sagittal sections

were obtained and H&E stained using standard protocols. For inner ears, heads were removed, skinned and bisected along the midline before fixation in 10% neutral buffered formalin (Surgipath), and subsequent processing as above.

***Linkage analysis***

DNA from the parental strains (C57BL/6J and C3H.C-*Pde6b*$^{+}$) and five affected G3 mice were scanned using an Illumina mouse low-density linkage array employing 271 informative SNPs.

***Mutational analysis of Map3k1***

Exons and the immediate flanking sequences of *Map3k1* were amplified from *goya*, C57BL/6J and C3H.C-*Pde6b*$^{+}$ genomic DNA employing oligonucleotides that were also used for Sanger sequencing.

***RT-PCR***

Total RNA was extracted from microdissected P1 organ of Corti using the RNeasy micro kit (Qiagen). For each sample RNA was pooled from four ears from 2 mice. First strand cDNA was synthesised using a high capacity cDNA reverse transcription kit (Life technologies) using a combination of oligo-(dT), random hexamer and *Map3k1* specific primers. The cDNA was then used as a template for PCR amplification using a forward primer spanning the end of exon 11 and the beginning of exon 12 and a reverse primer from exon 14 (Primer sequences on request). PCR products were separated by gel electrophoresis, bands excised, cloned into pGEM-T vector, and sequenced using SP6 and T7 primers.

***Gene Expression (Supplemental data figure S2)***

RNA extractions and cDNA synthesis were performed as described above, except that only random hexamers were used to prime the cDNA synthesis reactions. TaqMan® (Life Technologies) assays for *Ccna1 (Cyclin A1), Ccnd1 (Cyclin D1), Dhfr, Map3k1, Rb1, Col1a1, E2f1, fos, Jun, Axin2, CTNNB1 (B-catenin), Lgr5 and gapdh,* were run on a 7500 Fast real time PCR machine (Applied Biosystems) as per manufacturer's recommended instructions.

***Auditory Brainstem Response***

Auditory-evoked Brainstem Response (ABR) testing was performed as previously described by Hardisty-Hughes *et al.*, (Hardisty-Hughes et al., 2010). Tone burst stimuli were presented free-field at 8kHz, 12kHz, 20kHz and 26 kHz to the right ear of the mouse. TDT system III hardware and software (Tucker Davis Technology) was used for stimulus presentation and response averaging, starting at the highest level (90dB SPL) and reducing in 5 or 10dB increments until no response trace could be observed. Mice that displayed no response to a 90dB SPL stimulus were recorded as 100dB SPL for subsequent analysis.

***Scanning Electron Microscopy (SEM)***

Animals were euthanized and excised inner ears were fixed overnight in 2.5% Gluteraldehyde in 0.1M phosphate buffer (Sigma-Aldrich), then decalcified for 48 hours in 4.3% EDTA in 0.1M phosphate buffer (Sigma-Aldrich). Fine dissection was performed to reveal the organ of Corti, before osmium tetroxide (Agar Scientific) – thiocarbohydrazide (Fluka) (OTOTO) processing (adapted from (Hunter-Duvar, 1978)) was carried out. Samples were then dehydrated through increasing strength

ethanol solutions (Fisher Scientific) and critical point dried using an Emitech K850 (EM Technologies LTD). Specimens were then mounted on stubs using silver paint (Agar Scientific) and sputter coated with platinum using a Quorum Q150T sputter coater (Quorum Technologies). Prepared cochleae were visualised with a JEOL LSM-6010 (Jeol Ltd.) scanning electron microscope. Hair cell counts were performed by counting the number of adjacent IHC and OHC to 20 pillar cells, for the analysis the cochlea was divided into 4 separate regions (turns), apical (<90° from apex), mid apical (90-180° from apex), mid (180-360° from apex) and mid basal (360-540° from apex). Ears from at least 3 mice were analysed for each genotype at each turn and time point.

***X-Gal staining***

Mice were euthanized and inner ears removed and fixed for 2 hours at 4°C in 0.1M phosphate buffer containing 1% paraformaldehyde (Sigma-Aldrich) 2mM $MgCl_2$ (Sigma-Aldrich), 0.25% gluteraldehyde (Sigma-Aldrich) and 5mM EGTA (Merck Millipore). Ears were then washed in 0.1M phosphate buffer containing 2mM $MgCl_2$ (Sigma-Aldrich) and 0.02% NP-40 (Fluka). Staining was performed overnight at room temperature in a solution of 0.1M phosphate buffer containing 2mM $MgCl_2$ (Sigma-Aldrich), 5mM potassium ferrocyanide (Sigma-Aldrich), 5mM potassium ferricyanide (Sigma-Aldrich), 0.02% NP-40 and 1mg/ml 5-bromo-4-chloro-indolyl-β-D-galactopyranoside (X-Gal) (Sigma-Aldrich). Post-staining, ears were decalcified in 4.3% EDTA in 0.1M phosphate buffer (Sigma-Aldrich) for 48 hours at 4°C, before paraffin embedding and sectioning at 10µm. Sections and wholemount dissected cochlea were imaged on a Zeiss Axio Observer Z-1 microscope using extended focus image capture.

***Peggy Simple Western Size Assay***

Whole inner ears from three P1 mice (1 ear per mouse) were pooled and lysed in 20mM Bicene with 0.6% Chaps supplemented with phosSTOP™ and cOmplete mini™ inhibitor cocktails (Roche), using a Precellys 24 homogeniser with a soft tissue kit (Precellys).

Capillary based immunodetection was performed using the automated Peggy™ system (Simple Western™) as described previously (Siggers et al., 2014). Briefly, lysates were mixed with Simple Western™ sample dilution buffer (Protein Simple) containing reducing agent and fluorescent standards, and denatured at 95ºC for 5min. Samples were then loaded into the 384 well assay-plate and proteins were separated through size resolving matrix, immobilized to the inner capillary wall, incubated with p38 MAPK (CST9212), phospho-p38 MAPK (Thr180/Tyr182) (CST9215), p44/42 MAPK (ERK1/2) (CST9102), phospho-p44/42 MAPK (ERK1/2) (Thr202/Tyr204) (CST4377), SAPK/JNK (CST9252) and phospho-SAPK/JNK (Thr183/Tyr185) (CST9251) primary antibodies and HRP- conjugated secondary antibodies before detection using chemiluminescence.

***Immunohistochemistry***

**Phospho-p38, phospho-JNK and phospho-ERK1/2:**

P1 mice were euthanized by decapitation and bisected heads fixed in 4% PFA in PBS for 1 hour at 4°C. The bisected heads were then dehydrated and embedded in paraffin wax and 5µm sections collected onto charged slides. Sections were de-paraffinised, endogenous peroxidase activity quenched by submersion in 3% $H_2O_2$, washed in 1XTBST and blocked in 1XTBST containing normal goat serum. Sections were then

incubated overnight at 4°C with rabbit monoclonal anti-phospho p38 MAPK (Thr180/Tyr182) (Cell Signalling Technology) at 1:1500 dilution, phospho-p44/42 MAPK (ERK1/2) (Cell Signalling Technology) at 1:1000 dilution or phospho-SAPK/JNK (Thr183/Tyr185) (Cell Signalling Technology) at 1:1000 dilution. The VECTASTAIN® Elite ABC Rabbit IgG avidin biotin kit (Vector Laboratories) and DAB+ Chromagen (Dako) were used for detection. For anti- phospho-p38 labelled images, the ImmunoRatio plugin (http://jvsmicroscope.uta.fi/immunoratio/) for Image J (http://imagej.nih.gov/ij/) was used to quantify the percentage of positively stained nuclei.

**Proliferation detection and p27KIP1 immunofluorescence:**

The Click-iT Plus™ EdU Alexa Fluor 594 Imaging Kit (Life Technologies) was used to identify proliferating cells in embryonic cochlea. Pregnant females were injected with 100µg 5-ethynyl-2'-deoxyuridine (EdU) in 200µl PBS twice, at 2 hour intervals, before embryos were harvested 2 hours after final injection at either E14.5 or E18.5. Embryonic heads were fixed in 4% PFA in PBS for 1 hour at 4°C and tail collected for genotyping. Fixed heads were then dehydrated and embedded in paraffin wax and 5µm sections collected onto charged slides. The copper-azide 'click' Alexa Fluor 594 reaction for detection of EdU was performed as per the manufacturer's instructions, and processed slides were washed in PBS containing 3% BSA at RT. Slides were then blocked with 1XPBS containing 5% donkey serum and 0.5% Triton X-100 (Sigma), before incubation with rabbit polyclonal anti-p27KIP1 (Cell Signalling Technology) at 1:200 dilution overnight at 4°C. Slides were washed in PBS before incubation with Alexa Fluor 488 conjugated donkey anti-rabbit secondary antibody at 1:200 dilution.

Fluorescent confocal images were collected using a Zeiss LSM 700 inverted microscope.

***Statistical Analysis***

***Within-genotype rates of hair-cell loss across weeks 2, 4, and 9***

Counts were split into six distinct data sets for model fitting—according to hair cell type (inner or outer) and genotypic group. A Poisson generalized linear model was fitted to each data set separately. The model was specified as

$$\Pr(y_{twi} = k) = \frac{\exp(-\lambda_{twi})\lambda_{twi}^{k}}{k!} \quad , \qquad k = 0,1,2,...$$

$$\log \lambda_{twi} = \alpha_t + \beta_t \times (w-2)$$

(i.e. with a turn-specific, log-linear relationship between mean hair-cell count and week), where

- $t \in \{1,2,3,4\}$ indexes turn (1 = apical, 2 = mid-apical, 3 = mid, 4 = mid-basal),
- $w \in \{2,4,9\}$ denotes week,
- $i \in \{1,2,...,n_{tw}\}$ indexes mouse within (turn, week) group,
- $y_{twi}$ is the observed hair cell count in week *w*, at turn *t*, in mouse *i*, and
- $\lambda_{twi}$ is the mean hair cell count in week *w*, at turn *t*, in mouse *i*.

For estimates and confidence intervals for the weekly percentage change in mean hair cell count, at each turn *t* (i.e. $100 \times \left[\exp(\beta_t) - 1\right]$) see supplementary materials Table S1. Supplementary materials Table S2 displays p-values from testing the null hypothesis that the weekly percentage change is zero (i.e. $H_0 : \beta_t = 0$). Application of

a variety of diagnostic tools suggested that the model provided a reasonably good fit to the data.

Model fitting, diagnostic plots, and hypothesis tests were performed using the glm()-based functionality of the package "stats" in R (27)

***Inter-genotype comparison of hair cell counts at week 2***

For each cell type (inner and outer) and for each turn, cell counts were compared pair-wise between genotypic groups, p-values result from a Welch *t*-test applied to log-transformed hair cell counts.

***Comparison of qualitative phenotypes across genotypic groups***

The proportion of mice carrying each particular qualitative phenotype (Normal, Extra row or Extra OHC) was estimated in each genotypic group (*Map3k1*$^{+/+}$, *Map3k1*$^{goya/+}$ and *Map3k1*$^{tm1Yxia/+}$). Phenotype proportions were compared pair-wise across genotypes to determine whether mice with a particular phenotype were over-represented in some genotypic groups relative to others. Specifically, estimates and exact binomial confidence intervals were obtained for the proportion of mice of a particular genotype carrying a particular phenotype (28). Fisher's exact test was used to test the null hypothesis of equality of phenotypic proportion across a pair of genotypic groups (for estimates, confidence intervals, and p-values see supplementary material Table S3).

**Acknowledgements**

This work was supported by the Medical Research Council (MC_A390_5RX80 to SDMB). We thank the Wellcome Trust Clinical Research Facility at the Western General Hospital, Edinburgh for facilities and assistance with the genome scan. We would like to thank Ying Xia's group at the University of Cincinnati College of Medicine for the access to the *Map3k1*$^{tm1Yxia}$ mouse line. We would also like to thank the core facilities at the MRC Harwell Mammalian Genetics Unit and Mary Lyon Centre for their combined efforts.

**Competing Interests**

The authors declare no competing financial interests.

**Authors Contributions**

AP, SC, IJ, RH, MB & SB designed the study. AP, SC, RH, SM, GN, EC performed the experiments and data analysis. AP, SC, IJ, MB, SB prepared the manuscript. All authors read and approved the manuscript.

## References


**Deng, M., Chen, W. L., Takatori, A., Peng, Z., Zhang, L., Mongan, M., Parthasarathy, R., Sartor, M., Miller, M., Yang, J. et al.** (2006). A role for the mitogen-activated protein kinase kinase kinase 1 in epithelial wound healing. *Mol Biol Cell* **17**, 3446-55.

**Hardisty-Hughes, R. E., Parker, A. and Brown, S. D.** (2010). A hearing and vestibular phenotyping pipeline to identify mouse mutants with hearing impairment. *Nat Protoc* **5**, 177-90.

**Hunter-Duvar, I. M.** (1978). A technique for preparation of cochlear specimens for assessment with the scanning electron microscope. *Acta Otolaryngol Suppl* **351**, 3-23.

**Juriloff, D. M., Harris, M. J. and Dewell, S. L.** (2004). A digenic cause of cleft lip in A-strain mice and definition of candidate genes for the two loci. *Birth Defects Res A Clin Mol Teratol* **70**, 509-18.

**Loke, J., Pearlman, A., Radi, O., Zuffardi, O., Giussani, U., Pallotta, R., Camerino, G. and Ostrer, H.** (2013). Mutations in MAP3K1 tilt the balance from SOX9/FGF9 to WNT/β-catenin signaling. *Human molecular genetics*.

**Lowenheim, H., Furness, D. N., Kil, J., Zinn, C., Gultig, K., Fero, M. L., Frost, D., Gummer, A. W., Roberts, J. M., Rubel, E. W. et al.** (1999). Gene disruption of p27(Kip1) allows cell proliferation in the postnatal and adult organ of corti. *Proc Natl Acad Sci U S A* **96**, 4084-8.

**Mongan, M., Wang, J. C., Liu, H. S., Fan, Y. X., Jin, C., Kao, W. Y. W. and Xia, Y.** (2011). Loss of MAP3K1 enhances proliferation and apoptosis during retinal development. *Development* **138**, 4001-4012.

**Morrison, D. K.** (2012). MAP kinase pathways. *Cold Spring Harb Perspect Biol* **4**.

**Pearlman, A., Loke, J., Le Caignec, C., White, S., Chin, L., Friedman, A., Warr, N., Willan, J., Brauer, D., Farmer, C. et al.** (2010). Mutations in MAP3K1 cause 46,XY disorders of sex development and implicate a common signal transduction pathway in human testis determination. *Am J Hum Genet* **87**, 898-904.

**Sage, C., Huang, M., Karimi, K., Gutierrez, G., Vollrath, M. A., Zhang, D. S., Garcia-Anoveros, J., Hinds, P. W., Corwin, J. T., Corey, D. P. et al.** (2005). Proliferation of functional hair cells in vivo in the absence of the retinoblastoma protein. *Science* **307**, 1114-8.

**Sage, C., Huang, M. Q., Vollrath, M. A., Brown, M. C., Hinds, P. W., Corey, D. P., Vetter, D. E. and Chen, Z. Y.** (2006). Essential role of retinoblastoma protein in mammalian hair cell development and hearing. *Proceedings of the National Academy of Sciences of the United States of America* **103**, 7345-7350.

**Siggers, P., Carre, G. A., Bogani, D., Warr, N., Wells, S., Hilton, H., Esapa, C., Hajihosseini, M. K. and Greenfield, A.** (2014). A novel mouse Fgfr2 mutant, hobbyhorse (hob), exhibits complete XY gonadal sex reversal. *PLoS One* **9**, e100447.

**Takatori, A., Geh, E., Chen, L., Zhang, L., Meller, J. and Xia, Y.** (2008). Differential transmission of MEKK1 morphogenetic signals by JNK1 and JNK2. *Development* **135**, 23-32.

**Taylor, R. R., Jagger, D. J. and Forge, A.** (2012). Defining the cellular environment in the organ of Corti following extensive hair cell loss: a basis for future sensory cell replacement in the Cochlea. *PLoS One* **7**, e30577.

**Warr, N., Bogani, D., Siggers, P., Brixey, R., Tateossian, H., Dopplapudi, A., Wells, S., Cheeseman, M., Xia, Y., Ostrer, H. et al.** (2011). Minor abnormalities of testis development in mice lacking the gene encoding the MAPK signalling component, MAP3K1. *PLoS One* **6**, e19572.

**Xia, Y. and Kao, W. W.** (2004). The signaling pathways in tissue morphogenesis: a lesson from mice with eye-open at birth phenotype. *Biochem Pharmacol* **68**, 997-1001.

**Xia, Y., Makris, C., Su, B., Li, E., Yang, J., Nemerow, G. R. and Karin, M.** (2000). MEK kinase 1 is critically required for c-Jun N-terminal kinase activation by proinflammatory stimuli and growth factor-induced cell migration. *Proc Natl Acad Sci U S A* **97**, 5243-8.

**Yujiri, T., Ware, M., Widmann, C., Oyer, R., Russell, D., Chan, E., Zaitsu, Y., Clarke, P., Tyler, K., Oka, Y. et al.** (2000). MEK kinase 1 gene disruption alters cell migration and c-Jun NH2-terminal kinase regulation but does not cause a measurable defect in NF-kappa B activation. *Proc Natl Acad Sci U S A* **97**, 7272-7.

**Zhang, L., Deng, M., Parthasarathy, R., Wang, L., Mongan, M., Molkentin, J. D., Zheng, Y. and Xia, Y.** (2005). MEKK1 transduces activin signals in keratinocytes to induce actin stress fiber formation and migration. *Mol Cell Biol* **25**, 60-5.

**Zhang, L., Wang, W., Hayashi, Y., Jester, J. V., Birk, D. E., Gao, M., Liu, C. Y., Kao, W. W., Karin, M. and Xia, Y.** (2003). A role for MEK kinase 1 in TGF-beta/activin-induced epithelium movement and embryonic eyelid closure. *EMBO J* **22**, 4443-54.

## Figures

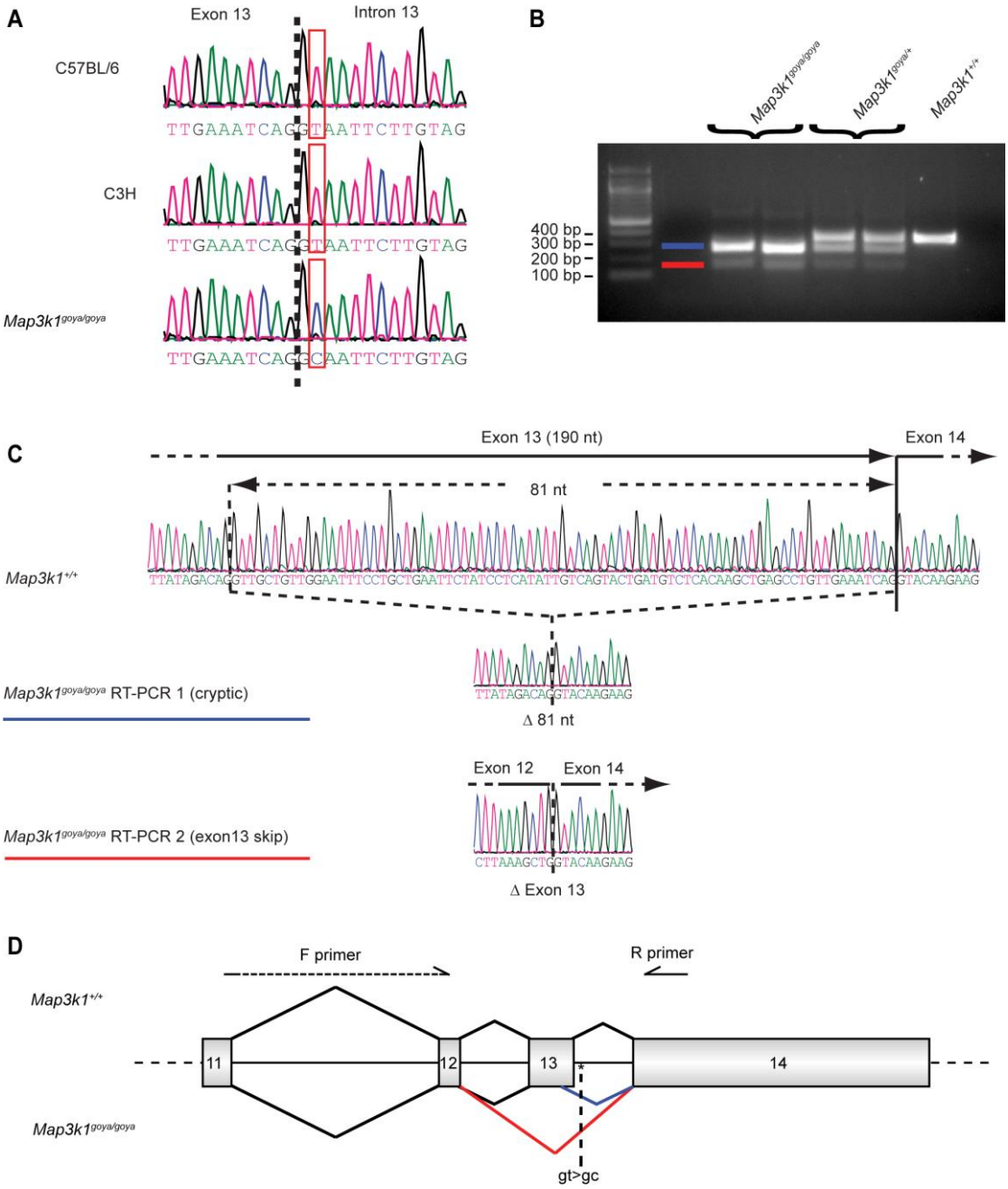


**Figure 1. *Map3k1* is mutated in *goya* mice.** (A) Genomic DNA sequence traces showing the *Map3k1* exon 13 donor splice site in the parental strains (C57BL/6 and C3H), and homozygous mutant (*Map3k1*$^{goya/goya}$) mice. The affected nucleotide is boxed (T in parental strains and C in *Map3k1*$^{goya/goya}$) and the exon/intron border is

indicated by the dashed line. (B) RT-PCR analysis of RNA extracted from the organ of Corti. For *Map3k1*$^{+/+}$, a single 341bp amplicon corresponding to the expected wild-type *Map3k1* sequence was observed. For *Map3k1*$^{goya/goya}$, no wild-type amplicon was observed, instead two smaller amplicons were identified (denoted by blue and red lines). All three amplicons were found for *Map3k1*$^{goya/+}$. (C) Sanger sequencing reveals aberrant splicing in *Map3k1*$^{goya/goya}$. i) sequencing of the single *Map3k1*$^{+/+}$ product confirms normal splicing of exons 12/13/14, ii) sequencing of the larger *Map3k1*$^{goya/goya}$ product (blue) reveals the use of a cryptic splice site within exon 13, resulting in an in-frame deletion of 81 nucleotides, iii) sequencing of the smaller *Map3k1*$^{goya/goya}$ product (red) reveals exon 12 splicing directly to exon 14, with complete skipping of exon 13. (D) Cartoon depicting the aberrant splicing events occurring in *Map3k1*$^{goya/goya}$ mice. Exons are depicted as numbered boxes, and the 'cryptic' and 'exon 13 skip' splicing events are shown as blue and red lines, respectively. The location of the *goya* mutation is shown.

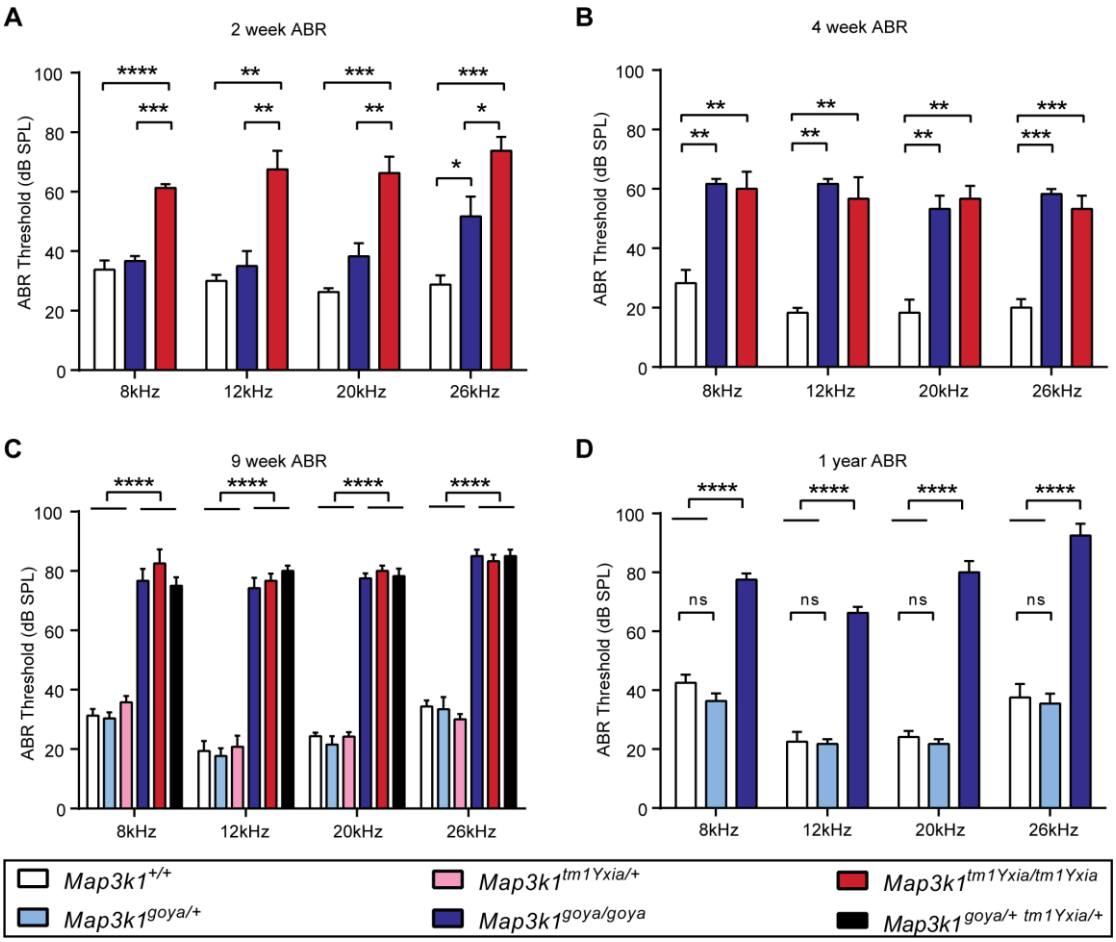


**Figure 2. Map3k1 deficient mice have a progressive hearing loss.**

(A) Average ABR thresholds of *Map3k1*$^{+/+}$(n=4), *Map3k1*$^{goya/goya}$ (n=3) and *Map3k1*$^{tm1Yxia/tm1Yxia}$ (n=4) mice at 2-weeks of age (P16). *Map3k1*$^{tm1Yxia/tm1Yxia}$ show significantly elevated thresholds at all frequencies when compared to wild-type or *Map3k1*$^{goya/goya}$ mice. *Map3k1*$^{goya/goya}$ mice only show a significant difference from wild-type at 26kHz. (B) At 4-weeks of age *Map3k1*$^{goya/goya}$ (n=3) and *Map3k1*$^{tm1Yxia/tm1Yxia}$ (n=3) mice have significantly elevated average ABR thresholds (+30-40dB) when compared to *Map3k1*$^{+/+}$ (n=3) mice across all frequencies tested. (C) By 9-weeks of age *Map3k1*$^{goya/goya}$ (n=6), *Map3k1*$^{tm1Yxia/tm1Yxia}$ (n=6) and *Map3k1*$^{goya/tm1Yxia}$ (n=6) mice exhibit severe hearing loss demonstrated by ABR thresholds 50 – 60dB above *Map3k1*$^{+/+}$ mice. Mice heterozygous for both the *goya*

(n=13) and *tm1Yxia* (n=6) alleles have thresholds not significantly different from wild-type at 9-weeks of age, showing that they do not suffer the same progressive hearing loss as homozygote mice. (D) ABR performed at 1-year of age show that *Map3k1*$^{goya/+}$ (n=6) mice have similar thresholds compared to *Map3k1*$^{+/+}$ (n=5) mice. Also, *Map3k1*$^{goya/goya}$ (n=7) mice have thresholds similar to those measured at 9-weeks of age suggesting no further decline in hearing function. Data shown are mean ± standard error of the mean, p values calculated using one-way ANOVA with TUKEY post hoc analysis - *p=<0.05, **p=<0.01, ***p=<0.001, ****p=<0.0001.

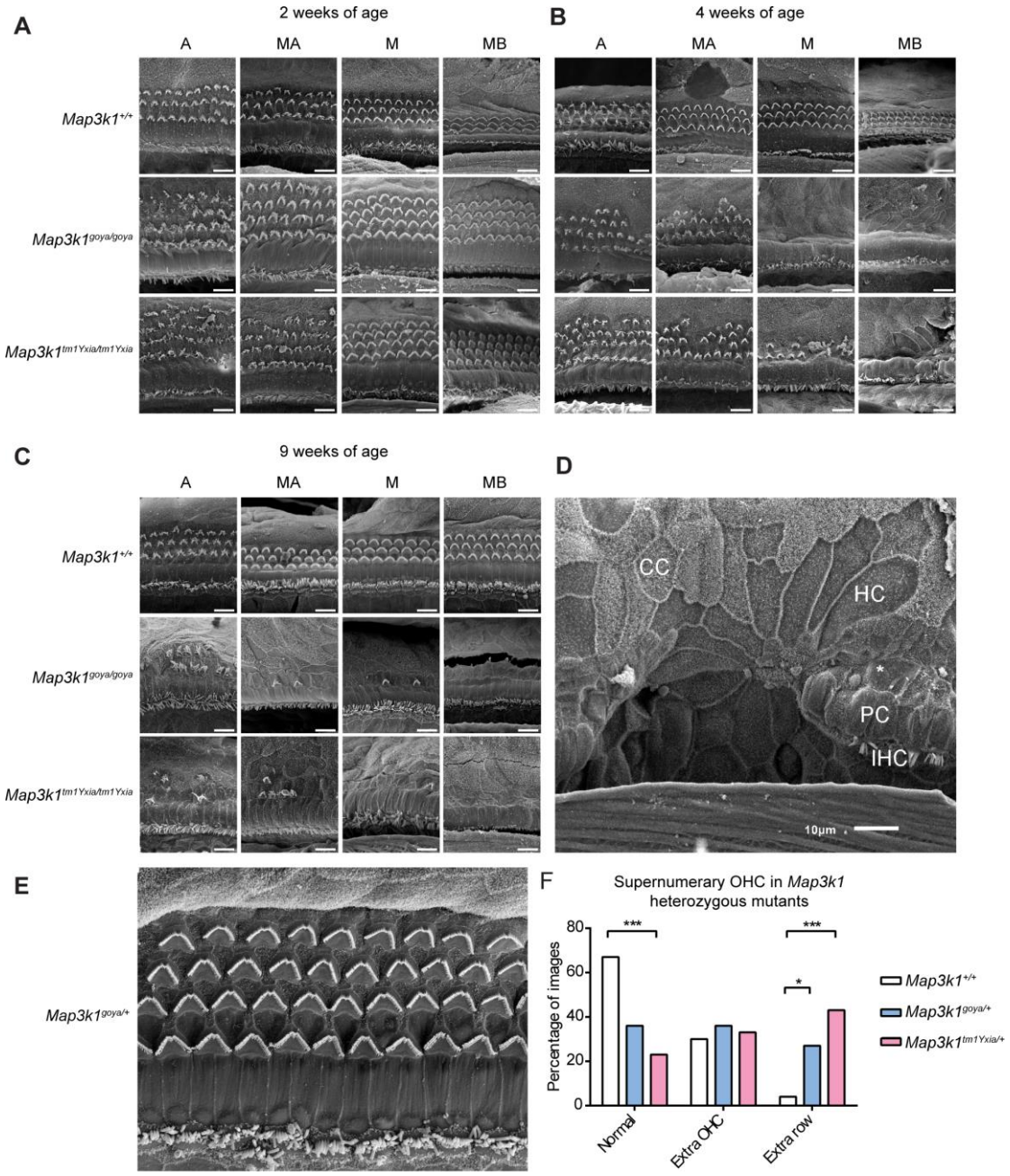


**Figure 3. Mice lacking functional MAP3K1 develop supernumerary OHC's and show progressive degeneration of OHCs.** (A-C) Representative scanning electron micrographs from the apical (A), mid-apical (MA), mid (M) and mid-basal (MB) turns of organ of Corti from +/+, *Map3k1*$^{goya/goya}$ (*goya/goya*) and *Map3k1*$^{tm1Yxia/tm1Yxia}$ (*tm1Yxia/tm1Yxia*) mice, at 2-, 4- and 9-weeks of age. Both *Map3k1*$^{goya/goya}$ and *Map3k1*$^{tm1Yxia/tm1Yxia}$ mice have an extra row of OHCs at 2-weeks of age. A progressive

loss of OHCs is seen between 2- and 9-weeks of age in both homozygous mutants, but not +/+ cochleae. An apical-to-basal increase in severity of degeneration was also observed. (D) Scanning electron micrograph demonstrating the rosette like cellular formation in a 9-week old *Map3k1*$^{tm1Yxia/tm1Yxia}$ mouse. The remains of some IHC stereocilia bundles can be seen (IHC), all OHC are missing (*) and pillar cells (PC) have been replaced in the rosette formation with Hensen (HC) and Claudius (CC) like cells (all scale bars represent 10µm). (E) Scanning electron micrograph showing an extra row of OHCs in the mid-basal region of a 9-week old *Map3k1*$^{goya/+}$ cochlea. (F) Clustered histogram representing the percentage of total images captured from *Map3k1*$^{+/+}$ (n=54), *Map3k1*$^{goya/+}$ (n=11) and *Map3k1*$^{tm1Yxia/+}$ mice (n=30), containing 3 rows of OHCs (normal), extra OHCs (1-4 OHCs in addition to the 3 normal rows), or extra rows of OHCs (≥ 5 OHCs in a continuous line, in addition to the 3 normal rows). Images of cochleae from both heterozygote alleles and *Map3k1*$^{+/+}$ mice showed isolated extra OHCs, however 27% of *Map3k1*$^{goya/+}$ and 43% of *Map3k1*$^{tm1Yxia/+}$ heterozygote images contained extra rows of OHCs, significantly higher than the 4% of *Map3k1*$^{+/+}$ images. The percentage of *Map3k1*$^{tm1Yxia/+}$ images containing the normal 3 rows of OHCs was also significantly lower when compared to *Map3k1*$^{+/+}$ (* $p<0.05$, *** $p<0.0001$, Fisher's exact test, see Materials and Methods and Supplementary materials Table S3 for estimates confidence intervals and p-values).

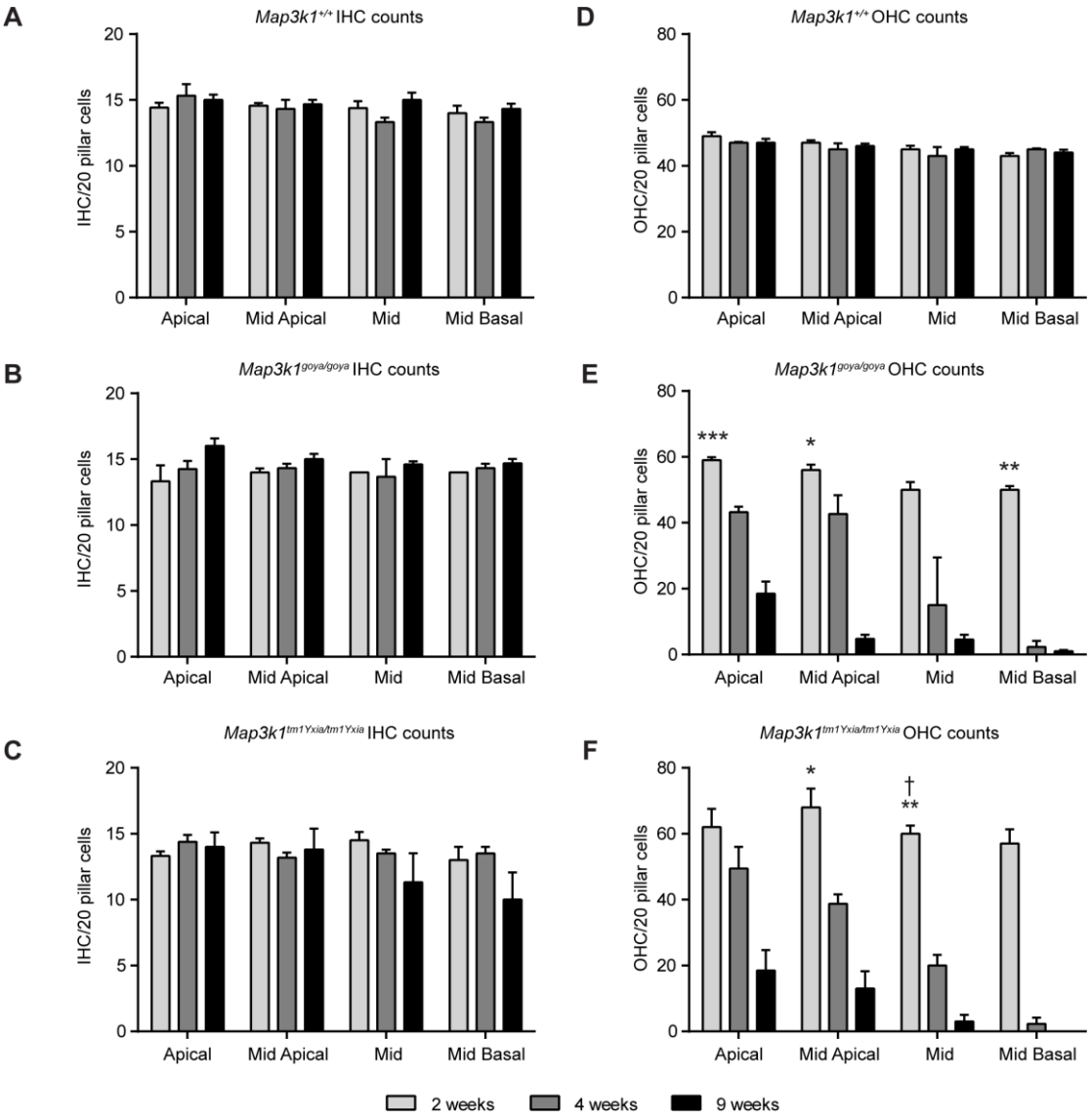


**Figure 4. Quantification of hair cell loss in the organ of Corti of *Map3k1*$^{goya/goya}$ and *Map3k1*$^{tm1Yxia/tm1Yxia}$ mice.** (A-C) Average number of IHC's in contact with 20 pillar cells at 2, 4 and 9-weeks of age. No significant differences in IHC number were observed in +/+ (A), *Map3k1*$^{goya/goya}$ (B), and *Map3k1*$^{tm1Yxia/tm1Yxia}$ (C) mice, although by 9-weeks of age reduced numbers of IHCs were observed in some of the *Map3k1*$^{tm1Yxia/tm1Yxia}$ cochleae. (D-F) Average number of +/+ (D), *Map3k1*$^{goya/goya}$ (E) and *Map3k1*$^{tm1Yxia/tm1Yxia}$ (F) OHCs in contact with 20 pillar cells at 2, 4 and 9-weeks of age. *t*-tests were performed to compare the mean numbers of OHCs between

genotypic groups at 2-weeks of age (see Methods). *Map3k1*$^{goya/goya}$ and *Map3k1*$^{tm1Yxia/tm1Yxia}$ mice have more OHCs than +/+. This difference was significant in the apical (***, p=<0.001), mid-apical (*=<0.05) and mid-basal turns (**, p<0.01) in *Map3k1*$^{goya/goya}$. In *Map3k1*$^{tm1Yxia/tm1Yxia}$ the extra number of OHCs was significantly higher than +/+ in the mid-apical (*, p<0.05) and mid (**, p<0.01) turns. In the mid turn of *Map3k1*$^{tm1Yxia/tm1Yxia}$ cochleae, significantly more OHCs were observed than in *Map3k1*$^{goya/goya}$ (†,<0.05), however there were no other obvious differences between the mutant alleles. By 4-weeks of age, nearly all *Map3k1*$^{goya/goya}$ and *Map3k1*$^{tm1Yxia/tm1Yxia}$ OHCs are missing in the mid-basal turn, and in the mid turn we observed variable levels of OHC loss in *Map3k1*$^{goya/goya}$ cochleae, and substantial loss in *Map3k1*$^{tm1Yxia/tm1Yxia}$ cochleae. In the mid-apical and apical turns OHC loss was evident but not to the extent of the mid and mid-basal turns. By 9-weeks of age the majority of OHCs are missing in the mid-basal and mid turns of both *Map3k1*$^{goya/goya}$ and *Map3k1*$^{tm1Yxia/tm1Yxia}$ cochleae, and severe loss is seen in the mid and mid-apical turns. No significant difference in OHC numbers were seen across the time points in +/+ cochleae. The rate of decrease in hair cell number over time was also analysed and found to be highly significant in both homozygous mutants (see Methods and Supplementary Table 1 and 2 for p values). Data shown are mean ± standard error of the mean, n ≥3 for genotype at each cochlear turn - *p=<0.05, **p=<0.01, ***p=<0.001.

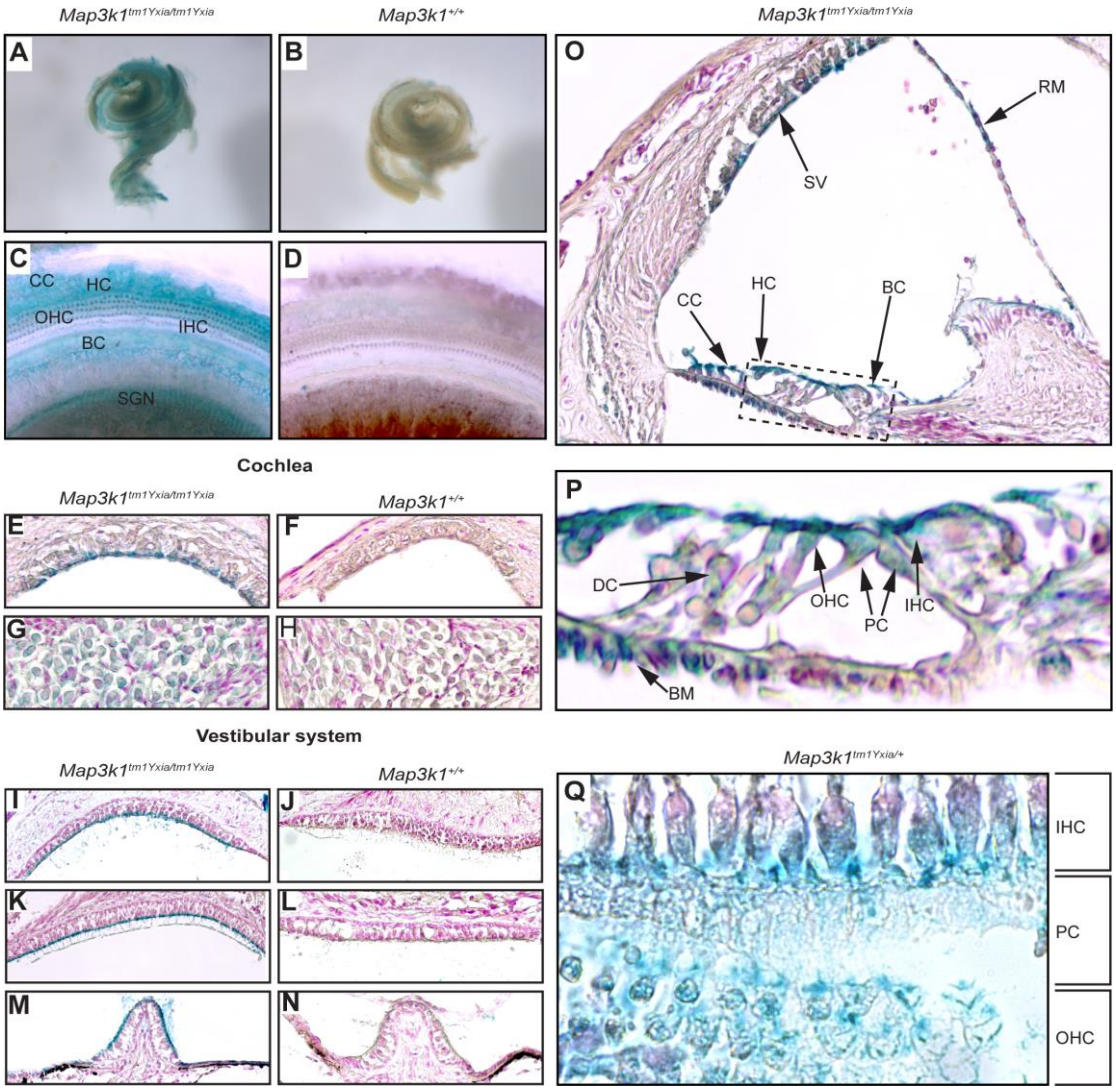


**Figure 5. Map3k1-ß-Galactosidase expression in the inner ear of P12 *Map3k1*$^{tm1Yxia/tm1Yxia}$ and *Map3k1*$^{tm1Yxia/+}$ mice.** Panels A and B show X-gal stained cochleae from *Map3k1*$^{tm1Yxia/tm1Yxia}$ and *Map3k1*$^{+/+}$ mice respectively. The *Map3k1*$^{tm1Yxia/tm1Yxia}$ cochlea (A) shows widespread staining due to the presence of a MAP3K1-ß-Galactosidase fusion protein in these mice. Panels C and D are extended focus images showing staining in the cochlear duct. In *Map3k1*$^{tm1Yxia/tm1Yxia}$ cochlea (C) strong staining can be observed in Claudius cells (CC), Hensen cells (HC), Outer Hair Cells (OHC), Inner Hair Cells (IHC), border cells of the internal spiral sulcus (BC) and spiral ganglion neurons (SGN). This staining is not observed in the

*Map3k1*$^{+/+}$ cochlea (D). Panels E-N show X-gal stained sagittal sections of the cochleae and vestibular systems from *Map3k1*$^{tm1Yxia/tm1Yxia}$ and *Map3k1*$^{+/+}$ mice: E,F - stria vascularis, G,H – spiral ganglion neurons, I,J – sacular macula, K,L – utricular macula, M,N – crista ampularis. X-gal positive staining is present in the marginal cells of the stria vascularis (E), the spiral ganglion neurons (G) and the apical surfaces of supporting cells and hair cells in all of the otolithic organs in the vestibular system of *Map3k1*$^{tm1Yxia/tm1Yxia}$ mice. Panel O shows the distribution of MAP3K1-ß-Galactosidase in the cochlear duct of *Map3k1*$^{tm1Yxia/tm1Yxia}$ mice. Staining is observed in the stria vascularis (SV), Reissner's membrane (RM), Claudius cells (CC), Hensen cells (HC) and border cells of the internal spiral sulcus (BC). Panel P is an enlargement of the organ of Corti (dashed box in panel O) and shows MAP3K1-ß-Galactosidase expression in the apical surface of IHC, OHC, Deiters' cells (DC), pillar cells (PC) and tympanic border cells of the basilar membrane (BM). Panel Q shows a transverse section of the organ of Corti from a *Map3k1*$^{tm1Yxia/+}$ mouse highlighting more clearly X-Gal positive staining in the IHCs, PCs and OHCs.

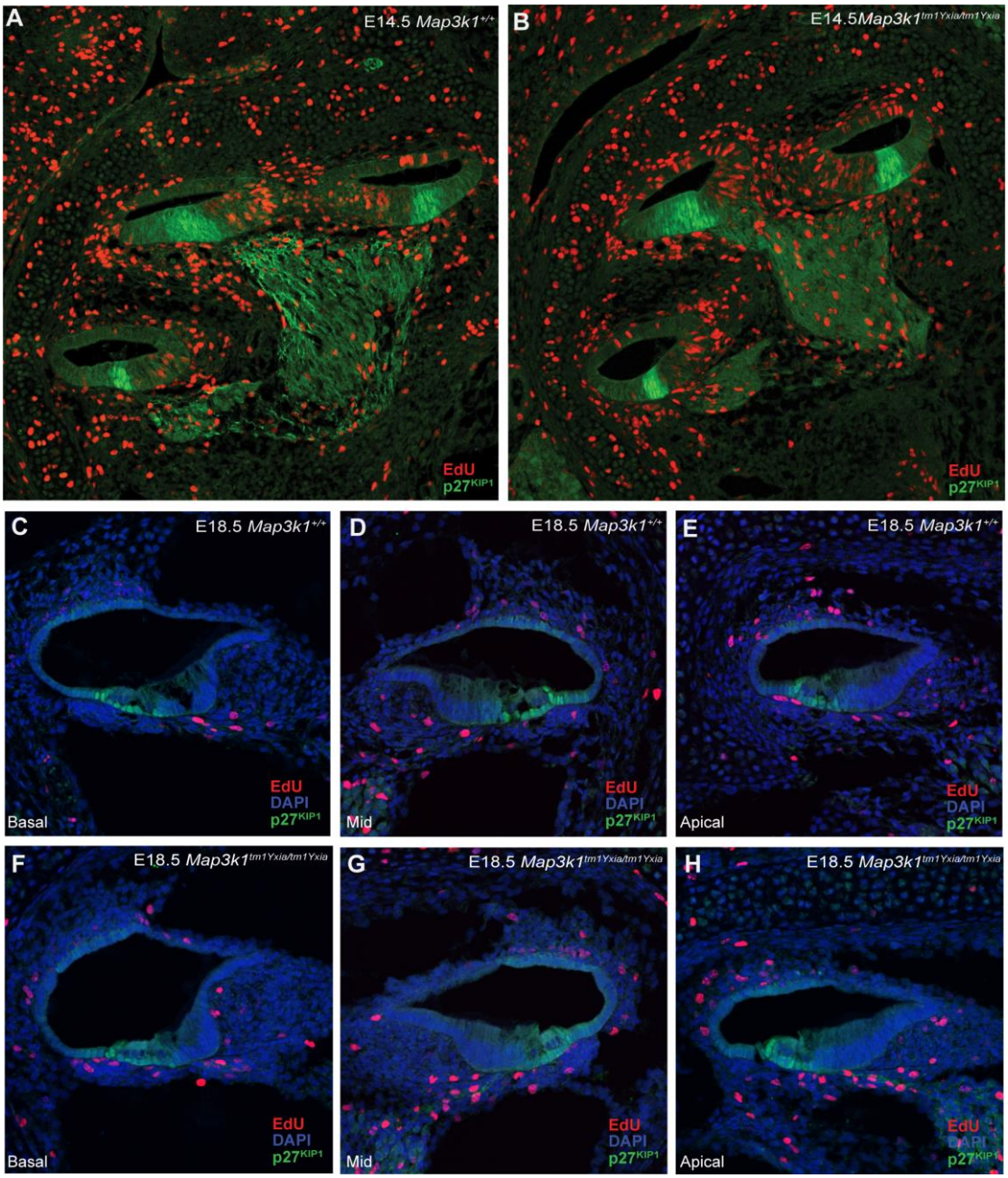


**Figure 6. Analysis of proliferation and p27KIP1 in the developing *Map3k1*$^{tm1Yxia/tm1Yxia}$ cochlea**. Immuno-detection of EdU-positive nuclei (red) and anti-p27KIP1 (green) and DAPI (to highlight nuclei in panels C-I). Pregnant females from timed matings were injected with EdU twice at 2hr intervals before embryos were harvested at E14.5 (A & B) or E18.5 (C-I). Localisation of p27KIP1 is unaffected in E14.5 *Map3k1*$^{tm1Yxia/tm1Yxia}$ and *Map3k1*$^{+/+}$ cochleae (A and B). The

absence of EdU positive nuclei in the region of p27KIP1 expression indicates the zone of non-proliferation is established correctly in *Map3k1*$^{tm1Yxia/tm1Yxia}$ mutant cochlea. At E18.5 we again saw no difference between the genotypes in p27KIP1 localisation, and found no evidence of proliferating cells as denoted by EdU positive nuclei in the cochlear duct epithelia in any of the cochlear turns (C-I).

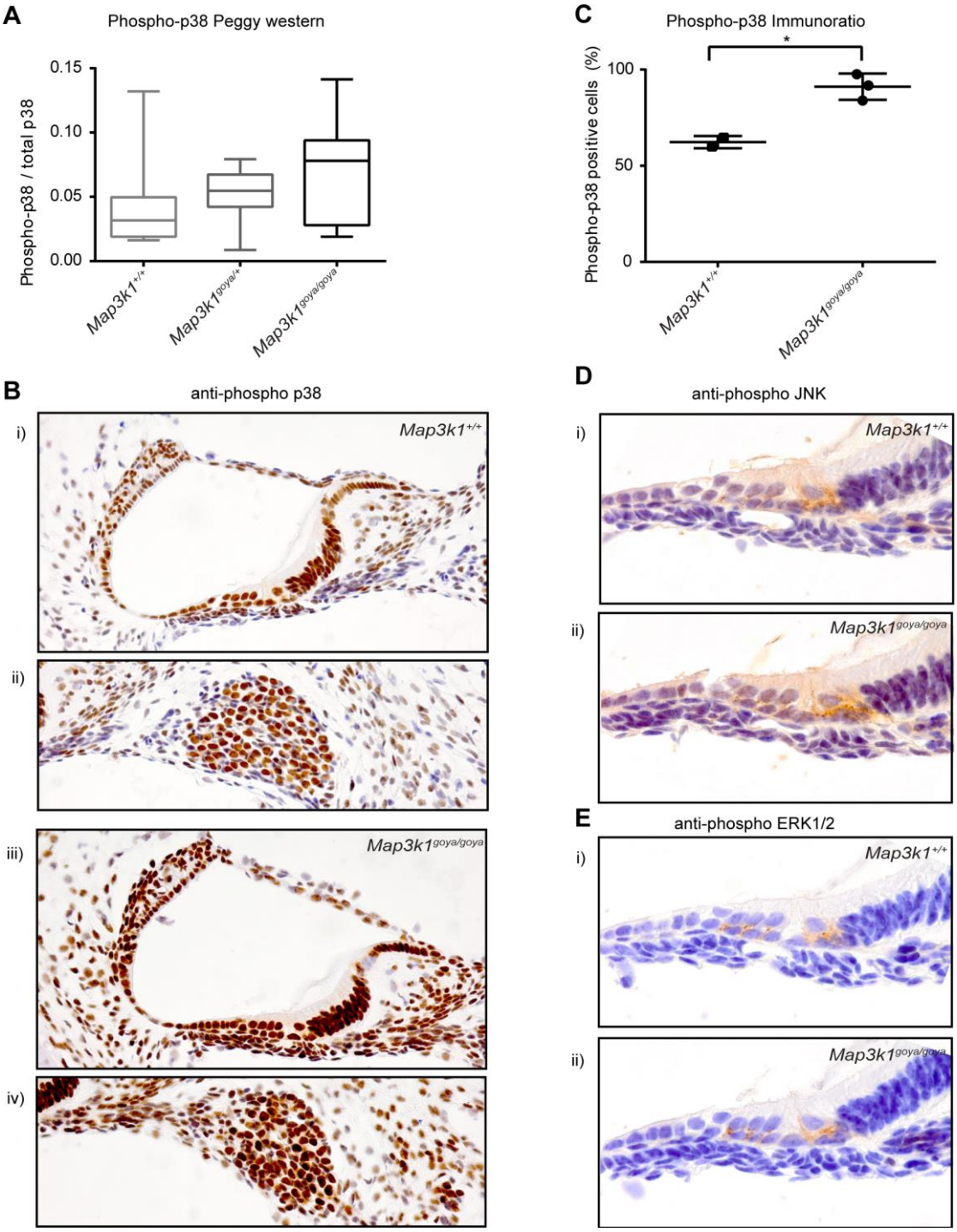


**Figure 7. The inner ears of P1 *Map3k1*$^{goya/goya}$ mice exhibit increased levels of p38 phosphorylation.** Panel A shows a box plot of the ratio of phosphorylated p38 to total p38 in *goya* inner ear total protein lysates from *Map3k1*$^{+/+}$, *Map3k1*$^{goya/+}$ and *Map3k1*$^{goya/goya}$ mice. Three ears (one each from separate mice) were pooled for each

lysate (number of lysates: *Map3k1*$^{+/+}$n=8, *Map3k1*$^{goya/+}$ n=7, *Map3k1*$^{goya/goya}$,n=8). A trend of increased p38 phosphorylation is observed in *Map3k1*$^{goya/goya}$ inner ear lysates when compared to *Map3k1*$^{+/+}$(p=0.282). Average *Map3k1*$^{goya/+}$ p38 phosphorylation levels appear intermediate between *Map3k1*$^{+/+}$ and *Map3k1*$^{goya/goya}$. Panels B-E) Immunohistochemical analysis of P1 *Map3k1*$^{goya/goya}$ cochlea confirms the increased level of p38 phosphorylation observed in the Peggy western data. Panels B i & iii show phosphorylated p38 expression in the mid turn of the cochlea of P1 *Map3k1*$^{+/+}$ (i) and *Map3k1*$^{goya/goya}$ (iii) mice. Widespread nuclear expression is seen in both genotypes, however, the depth of staining is greatly increased in *Map3k1*$^{goya/goya}$. Some nuclei in spiral ligament, spiral limbus and basilar membrane in the *Map3k1*$^{+/+}$ organ of Corti remained unstained with this length of chromogenic exposure. These results were consistent for littermate controls (*Map3k1*$^{+/+}$ n=2 *Map3k1*$^{goya/goya}$ n=3). Immunoratio was used to quantify the percentage of nuclei stained in each mid turn image (C & sup data). This analysis showed that the *Map3k1*$^{goya/goya}$ mice (n=3) had significantly increased numbers of positively stained cells when compared to *Map3k1*$^{+/+}$ (n=2). B ii and iv show increased positive staining for phosphorylated p38 in the spiral ganglion neurons of *Map3k1*$^{goya/goya}$ (iv) mice compared to *Map3k1*$^{+/+}$ (ii). Panels D and E show immunostaining of P1 organ of Corti using anti-phospho JNK and anti-phospho ERK1/2 antibodies respectively. No differences can be seen between *Map3k1*$^{+/+}$ (D i & E i) or *Map3k1*$^{goya/goya}$ (D ii & E ii) mice, although interestingly expression of both proteins is mainly observed below the basal surface of inner and outer hair cells, in contrast to the widespread nuclear expression of phosphorylated p38.

## Translational Impact

*Clinical issue*

In mammals, hearing loss arising from damage to inner ear sensory hair cells is, at present, irreversible. As such, there is currently much interest in the potential of using regenerative based therapies to restore hearing function, either through manipulation of any remaining hair cells causing them to re-enter the cycle cell and proliferate, or by inducing trans-differentiation of supporting cells into hair cells.

Over the last three decades, investigations of mouse mutants have helped reveal many genes and pathways required for hearing and cell specification in the cochlea. Indeed, the benefit of genetic standardization and the advantage of being able to image the murine inner ear, mean the mouse continues to be an excellent model organism for auditory research.

*Results*

In this study, the authors report the goya mouse model that carries an ENU-induced mutation in the Map3k1 gene. In addition to a previously reported eyes-open-at-birth phenotype, homozygote goya (and homozygous Map3k1 null) mice also have an auditory phenotype. At 2-weeks of age, homozygote goya mice have supernumerary outer hair cells, and have hearing thresholds similar to wild-type animals. By 9-weeks of age, these sensory cells have degenerated and the mice exhibit a severe hearing loss. Interestingly, heterozygous goya mice also develop supernumerary outer hair cells, but they do not progressively degenerate nor do these mice develop hearing loss. Supernumerary hair cells can result from aberrant proliferation of progenitor cells in the developing cochlea. However no increase in the number of proliferating (EdU positive) cells was observed, and the p27KIP1-defined zone of non-proliferation

appeared correctly established, in the embryonic cochleae of E14.5 Map3k1tm1Yxia/tm1Yxia mice. Studies into the expression level and phosphorylation status of known MAP3K1 target proteins showed no significant differences. However, an increase in p38 phosphorylation was observed in P1 goya inner ears when compared with wild-type controls.

*Implications and future directions*

For the first time, the goya mouse mutant introduces MAP3K1 as a key regulator of cochlear development and hair cell survival. This model has the potential to inform upon genes and pathways required for hearing. Indeed, it is interesting that MAP3K1 is known to regulate many of the genes and proteins currently being investigated for their efficacy in regenerative therapy. However, it is apparent that the exact mechanism by which MAP3K1 performs theses distinct roles is highly complex, and will require further investigation.